Electroabsorption Modulated Laser With High Immunity to Residual Facet Reflection

Oh Kee Kwon, Yong Soon Baek, and Yun C. Chung, *Fellow, IEEE*

***Abstract*— We report on the design for an electroabsorption-modulated laser (EML) that can provide a high immunity to the optical signal reflected from its output facet without any fabrication complexity and performance compromise. In particular, we theoretically investigate the effects of residual facet reflection on the static and dynamic performances of the high-speed EMLs. For this analysis, an accurate and consistent time-domain transfer-matrix-based laser model is developed. Based on this model, we perform the steady-state and large-signal analyses for the EML with finite facet reflectivities. The simulation result indicates that the EML with a high-gain compression factor is capable of reducing the power fluctuation and facet reflection-induced chirp under large-signal modualtion. Thus, it is desirable to design for increasing the damping of a distributed feedback (DFB) laser to realize the EML with a high immunity to this facet reflection. The simulation also shows that the effect of this facet reflection strongly depends on the phase condition between the optical signal reflected from the output facet and the light emitted from the DFB laser and, in particular, at that specific phase condition, a clear eye opening appears even at the relatively high-output facet reflectivity (i.e., $R_f = 1\%$).**

***Index Terms*— Distributed feedback (DFB) laser, electroabsorption modulator (EAM), electroabsorption-modulated laser (EML), large-signal modulation, residual facet reflection, time-domain transfer matrix model.**

I. Introduction

ELECTROABSORPTION modulated lasers (EMLs) have many advantages including the compactness, low cost, low power consumption and the integratability with other optical devices such as the monitoring photodetector, semiconductor optical amplifier, and couplers. The EML has been widely used as a 10-Gb/s optical transmitter for the intermediate-reach (i.e., 40 km) and long-reach (i.e., 80 km) applications as well as a 40-Gb/s transmitter for the very-short-reach (i.e., 2 km) application. Recently, there have also been many interests in utilizing the 4-channel EML array (each operating at 25 Gb/s) as an optical transmitter in the 100-Gb/s Ethernet system with the maximum reach of up to 40 km [1], [2]. For the use of EML in these applications, a clear eye opening even under a large-signal modulation should be provided. However, a reflected optical signal from the output facet of EML can perturb the lasing condition of a distributed feedback (DFB) laser, which, in turn, causes unwanted power fluctuations and a large chirp of the output signal under modulation [3]. It has been recently reported that this facet reflection can also cause a large peak or valley in the frequency response [4]–[6] and degrade the signal quality [6]. This problem is a critical issue for the design of a high-speed EML, since it frequently occurs in a DFB laser integrated with a short electroabsorption modulator (EAM). There are several chirp-reduction methods commonly used to avoid such an influence in the EML [4], [7]–[9]. For example, it has been reported that the facet reflection-induced chirp (i.e., DFB chirp) can be reduced by decreasing the reflectivity of the output facet to less than $\sim 2\times 10^{-4}$[7]. However, it is difficult to decrease the reflectivity to such a low value without utilizing a window structure [8] or a tilted waveguide [4] and accurately controlling the thickness of the dielectric coating materials. This influence can also be alleviated by realizing DFB lasers with high immunity to an external feedback (i.e., high κL DFB laser and complex-coupled (CC) DFB laser) [9]. However, in spite of their improvement in the reflection immunity, this method is still debatable since the use of high κL DFB lasers can result in the reduction of output power and the degradation of single-mode stability due to the longitudinal spatial hole-burning (LSHB) [10], and that of CC DFB lasers can make it much harder to control the lasing wavelength accurately. On the other hand, from an operational point of view, it is well-known that this influence can be suppressed by increasing the bias voltage of an EAM. This is equivalent to a decrease in the detuning between the lasing wavelength of a DFB laser and the absorption peak wavelength of an EAM. In this case, however, the output power is reduced due to the increase of the absorption of the EAM.

Considering all the methods described above, it is extremely difficult to design the EML having the capability of suppressing this influence without increasing fabrication complexities and/or compromising other important performances such as the output power, single-mode stability, and wavelength controllability. Nevertheless, we note that the power

Manuscript received April 23, 2012; revised June 17, 2012; accepted June 25, 2012. Date of publication June 29, 2012; date of current version July 17, 2012.

O. K. Kwon is with the Department of Electrical Engineering, Korea Advanced Institute of Science and Technology, Daejeon 305-701, Korea, and also with the Photonic-Wireless Convergence Components Research Department, Convergence Components and Material Research Laboratory, Electronics and Telecommunications Research Institute, Daejeon 305-700, Korea (e-mail: okkwon@etri.re.kr).

Y. S. Baek is with the Photonic-Wireless Convergence Components Research Department, Convergence Components and Material Research Laboratory, Electronics and Telecommunications Research Institute, Daejeon 305-700, Korea (e-mail: yongb@etri.re.kr).

Y. C. Chung is with the Department of Electrical Engineering, Korea Advanced Institute of Science and Technology, Daejeon 305-701, Korea (e-mail: ychung@ee.kaist.ac.kr).

Color versions of one or more of the figures in this paper are available online at http://ieeexplore.ieee.org.

Digital Object Identifier 10.1109/JQE.2012.2206799

and wavelength of the output signal are fluctuated with the maximum magnitude at the relaxation oscillation frequency of the DFB laser under this facet reflection and, in principle, this resonance depends on the device parameters and operational condition. In this respect, it may be possible to reduce such fluctuations by weakening the relaxation oscillation, which can be achieved by increasing the damping effect of a DFB laser. This design concept is somewhat different from that of the directly modulated DFB laser for high-speed operation since this damping effect can decrease a direct modulation bandwidth [11]. Thus, in this paper, we intend to verify our proposal and identify its effectiveness by systematically investigating the effects of the residual reflection on the device performances of EML. For this investigation, an accurate large-signal model capable of describing both the intensity and phase of the optical signal in the integrated laser is required. Various time-domain laser models, based on coupled-wave equation and carrier rate equation, have been reported [12]–[15]. For example, B. Kim has proposed a split-step time-domain model (SS-TDM) to improve the problem of L. M. Zhang's model [12] (which exhibits a large error and instability in the output power when the Bragg condition is deviated) by satisfying the energy conservation of the temporally changed slowly varying waves compulsorily [13]. However, since this model utilizes the fast numerical convergence without any appropriate estimations of the wavelength shift caused by the lasing condition changes, it is insufficient to describe the properties of the EML precisely.

M. G. Davis has proposed a time-dependent transfer matrix method (TD-TMM) and analyzed the dynamic properties of the multielectrode DFB lasers [14]. In his model, the dynamic wavelength shift (i.e., chirp) is considered to be caused by the deviation from Bragg condition and the shift of the Bragg wavelength itself under the direct modulation. The deviation from Bragg condition can be obtained from the minimum condition of the element (2, 2) of the overall transfer matrix including the laser structure, while the shift of the Bragg wavelength itself (due to LSHB) can be found from the change of the average value in the carrier density distribution. Estimating from the fact that the zero condition of the element (2, 2) of the overall transfer matrix is the same as the lasing condition of the perfect open resonator, it is reasonable to extract the dynamic wavelength shift from the minimum condition since the change of the element (2, 2) of the overall transfer matrix corresponds to the variation of the lasing condition under the modulation. Y. Kim has reported a complete large-signal model for the EML by combining Zhang's chirp model (i.e., EAM chirp) and Davis's model (i.e., DFB chirp) to describe the dynamic properties of the 10-Gb/s EML [15]. This model shows similar results between the calculation and the measurement in the output power and chirp for various bias voltages. However, the fluctuations of the calculated output power and chirp are considerably underestimated (i.e., Fig. 10 in [15]). In addition, the validity of the Davis's model (i.e., using the minimum condition of the element (2, 2) of the overall transfer matrix) is limited to the open resonator with zero reflectivities at both facets [16]. Thus, in this paper, we develop a large-signal model

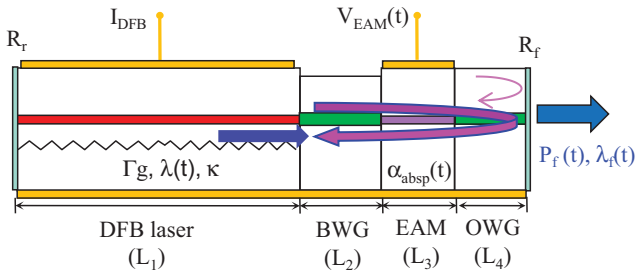

Fig. 1. Schematic diagram of an EML. I_{DFB} and $V_{EAM}(t)$ are the current injected into DFB laser and the voltage applied to the EAM, respectively. $P_f(t)$ and $\lambda_f(t)$ denote the power and the wavelength of output signal, respectively.

for the EML having non-zero facet reflectivities. For this purpose, we first develop an accurate time-domain laser model based on our previous time-independent transfer-matrix-based laser model [17]. In this model, the dynamic wavelength shift involves the temporal change of the lasing condition along the cavity and the instantaneous phase change of the output field under modulation. The former is obtained from the minimum condition of the Wronskian term (i.e., the determinant of the overall transfer matrix) for the structure and the latter by differentiating the phase of the complex slowly varying wave at the output facet. Unlike the Davis's model, the shift of the Bragg wavelength caused by LSHB is considered without any additional modeling in this model because the transfer matrices of the DFB region contain the refractive index change caused by the non-uniform carrier distribution along the cavity. In addition, this model enables us to analyze the static and spectral properties by using the (nominal) zero condition of the Wronskian term under the CW condition, as in our previous steady-state model. Based on this model, we investigate the effects of the residual reflection on the device performances by analyzing the static and large-signal performances of the EMLs for various parameters and conditions. The simulation result indicates that the EML having a high gain compression factor is capable of reducing the power fluctuation and facet reflection-induced chirp under the large-signal modualtion. In addition, using this model, we find several distinctive features including the effects of the interference between the optical signal reflected from the output facet and the light emitted from the DFB laser, the damping effect in high κL structure, and the operating condition insensitive to this facet reflection.

The rest of this paper is organized as follows. In Section II, the theoretical time-domain transfer-matrix-based laser model of the EML is described in details. The simulated results obtained by using this model are shown in Section III. Finally, this paper is summarized in Section IV.

II. Device Structure and Theoretical Model

Fig. 1 shows a schematic diagram of the EML analyzed in this paper. The device consists of a $\lambda/4$-shifted DFB laser, a bridge waveguide (BWG), an EAM, and an output waveguide (OWG). The BWG is used for the electrical isolation between the DFB laser and EAM and for the prevention of the degradation in frequency response by the photo-generated carrier accumulation in the isolation region in between the DFB laser

and EAM [18], [19]. The OWG can be used for realizing the tilted waveguide for additional reduction of output facet reflectivity or the spot-size converter for the improvement of fiber coupling efficiency.

The optical light reflected from this facet is coupled back into the DFB laser between the on and off states of the EAM, which can lead to perturb the lasing condition of a DFB laser. To examine such an effect in this integrated laser, we have developed a time-domain transfer-matrix-based laser model composed of various longitudinal regions. To consider the LSHB, we divided each region into small sections of length Δz and assumed all variables in each section to be constant. In EAM region, the changes of absorption coefficient $\alpha_{absp}(t)$ and refractive index $\Delta n_{absp}(t)$ as a function of the applied voltage $V_{EAM}(t)$ are considered. In this model, we neglected the thermal effect, noise characteristics, and electrical parasitics including the RF property of an EAM [20] and the bonding-wire [21].

A. Time-Domain Transfer-Matrix-Based Laser Model

The electric field in this laser can be approximated by

$$E(t,x,y,z) = E_0(x,y)\left[F(t,z)e^{-j\beta_0 z} + B(t,z)e^{j\beta_0 z}\right]e^{j\omega_0 t} \tag{1}$$

where $E_0(x,y)$ is the electric field of the guided-mode which depends mainly on the waveguide structure, and F(t, z) and B(t, z) are the time-dependent slowly varying forward and backward propagating waves along the longitudinal direction z, respectively. In addition, β_0 and ω_0 are the propagation constant and the angular frequency at a Bragg wavelength of λ_B.

Fig. 2 shows the schematic diagram of a time-domain transfer-matrix-based model and the relation between F(t, z) and B(t, z) within the section of Δz during the time interval of Δt. In this model, assuming that the medium remains unchanged over Δt and the group velocity is constant, F(t, z) and B(t, z) from $z = 0$ to $z = L$ at t_o and $t_o + \Delta t$ are related by the transfer matrices expressed by

$$\begin{bmatrix} F(t_0+\Delta t, z=L) \\ B(t_0, z=L) \end{bmatrix} = [T(t_0, L)] \begin{bmatrix} F(t_0, z=0) \\ B(t_0+\Delta t, z=0) \end{bmatrix} \tag{2}$$

where $[T(t_0, L)]$ is the overall transfer matrix at $t = t_0$. $[T(t, L)]$ can be written as follows:

$$[T(t,L)] = \prod_{j=o+1}^{p} [T_4(t,j)][D_3] \prod_{j=n+1}^{o} [T_3(t,j)][D_2] \prod_{j=m+1}^{n} [T_2(t,j)][D_1] \prod_{j=l+1}^{m} [T_1(t,j)][P] \prod_{j=1}^{l} [T_1(t,j)] \tag{3}$$

where $[T_i(t_0, j)]$ is the transfer matrix of the j $(= 1, 2, \ldots, p)$ section of the i region at $t = t_0$, and subscript i $(= 1, 2, 3, 4)$ stands for DFB laser, BWG, EAM, and OWG, respectively. In addition, [D] is a matrix representing the reflection induced by the refractive index difference between the regions and

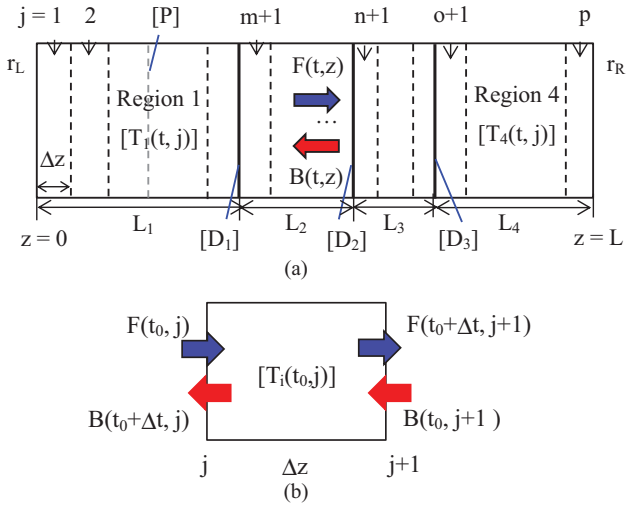

Fig. 2. (a) Schematic diagram of the time-domain transfer-matrix-based laser model and (b) relationship between F(t, z) and B(t, z) within the section length of Δz during a time interval of Δt. $[T_i(t_0, j)]$ is the transfer matrix of the j section of the i region at $t = t_0$.

[P] is the matrix representing the phase shift of DFB laser. $[T_i(t, j)]$ can be written as follows:

$$[T_i(t,j)] = \begin{bmatrix} T_{11}i(t,j) & T_{12}i(t,j) \\ T_{21}i(t,j) & T_{22}i(t,j) \end{bmatrix} \tag{4}$$

where

$$T_{11i}(t,j) = \cosh(\gamma_i(t,j)\Delta z) + \frac{\alpha_i(t,j) - j\delta_i(t,j)}{\gamma_i(t,j)} \sinh(\gamma_i(t,j)\Delta z) \tag{5-1}$$

$$T_{12_i}(t,j) = -\frac{j\kappa_i}{\gamma_i(t,j)} \sinh(\gamma_i(t,j)\Delta z)\, e^{-j\Omega} \tag{5-2}$$

$$T_{21i}(t,j) = \frac{j\kappa_i}{\gamma_i(t,j)} \sinh(\gamma_i(t,j)\Delta z)\, e^{j\Omega} \tag{5-3}$$

$$T_{22i}(t,j) = \cosh(\gamma_i(t,j)\Delta z) - \frac{\alpha_i(t,j) - j\delta_i(t,j)}{\gamma_i(t,j)} \sinh(\gamma_i(t,j)\Delta z) \tag{5-4}$$

$$\gamma_i(t,j)^2 = (\alpha_i(t,j) - j\delta_i(t,j))^2 + \kappa^2 \tag{6}$$

$$\alpha_i(t,j) = (\Gamma_i g(t,j) - \alpha_i - \Gamma_i \alpha_{absp}(t))/2 \tag{7}$$

$$\delta_i(t,j) = \frac{2\pi}{\lambda(t)} n_{eff,i}(t,j) - \beta_0 \tag{8}$$

where $\alpha_i(t, j)$ and $\delta_i(t, j)$ denote the amplitude gain and detuning from the Bragg condition, respectively; κ and Ω are the coupling coefficient and initial grating phase of the DFB region; Γ_i and α_i are the optical confinement factor and optical loss of each region; g(t, j) is the material gain of a DFB laser; and $\alpha_{absp}(t)$ is the material absorption coefficient of an EAM. $[D_i]$ can be written as follows:

$$[D_i] = \begin{bmatrix} \frac{n_{eff,i+1}(j+1)+n_{eff,i}(j)}{2n_{eff,i+1}(j+1)} & \frac{n_{eff,i+1}(j+1)-n_{eff,i}(j)}{2n_{eff,i+1}(j+1)} \\ \frac{n_{eff,i+1}(j+1)-n_{eff,i}(j)}{2n_{eff,i+1}(j+1)} & \frac{n_{eff,i+1}(j+1)+n_{eff,i}(j)}{2n_{eff,i+1}(j+1)} \end{bmatrix}. \tag{9}$$

When we know all spatial field distributions at $t = t_o$, the field distributions at $t = t_o + \Delta t$ can be obtained consecutively by

$$B(t_o+\Delta t, j) = \frac{B(t_o, j+1) - T_{i,21}(t_o, j)F(t_o, j)}{T_{i,22}(t_o, j)} \tag{10}$$

$$F(t_o + \Delta t, j+1) = T_{i,11}(t_o, j)F(t_o, j) + T_{i,12}(t_o, j)B(t_o + \Delta t, j) \quad (11)$$

where F($t_o + \Delta$t, z = 0) and B($t_o + \Delta$t, z = L) can be obtained by the boundary conditions:

$$F(t_0 + \Delta t, z = 0) = r_L B(t_0 + \Delta t, z = 0) \quad (12)$$

$$B(t_0 + \Delta t, z = L) = r_R F(t_0 + \Delta t, z = L) \quad (13)$$

where r_L and r_R are the reflection coefficient at z = 0 and z = L, respectively.

In a semiconductor laser, g(t, j) and $n_{eff,i}$(t, j) are varied with the carrier density N(t, z), photon density S(t, z) (= |F(t, z)|^2 + |B(t, z)|^2), and a lasing wavelength of λ(t). According to [17] and [22]–[24], they can be modeled as follows:

$$g_i(\lambda, N, S) = \frac{a_0(N(t,z) - N_0) - a_1[\lambda(t) - (\lambda_{p0} - a_2(N(t,z) - N_0))]^2}{1 + \varepsilon(t,z)} \quad (14)$$

$$n_{eff,i}(\lambda, N) = n_{eff0,i} + \frac{(n_{eff,i}(N(t,z)) - n_g)}{\lambda_B}(\lambda(t) - \lambda_B) - \frac{\alpha_H \Gamma_i \lambda(t) a_0}{4\pi} N(t,z) + \Gamma_i \Delta n_{absp}(t) \quad (15)$$

where a_0, a_1, and a_2 are the linear differential gain, gain curvature, and differential peak wavelength, respectively; N_0 is the transparent carrier density; λ_{p0} is the gain-peak wavelength at transparency; and ε is the gain compression factor. In (15), the first term $n_{eff0,i}$ represents the effective refractive index without a carrier injection. The second and the third terms indicate the dispersion property of the cavity and the refractive index change caused by the carrier injection, respectively, n_g is the group refractive index, and α_H is the linewidth enhancement factor. The fourth term represents the modal refractive index change induced by the variation of the absorption in the EAM.

Under a uniform injection current I_{DFB}, the carrier distribution at t = t_o + Δt can be obtained through a time-dependent rate equation as

$$\frac{dN(t,z)}{dt} = \frac{\eta I_{DFB}}{eV} - \frac{N(t,z)}{\tau_e(t,z)} - v_g g\,(\lambda(t), N(t,z), S(t,z))\, S(t,z) \quad (16)$$

where η the injection efficiency, e is the electron charge, V is the volume of the active region, τ_e(t, z) (= $A + BN$(t, z) + CN(t, z)^2)$^{-1}$ is the carrier lifetime, where A, B, and C are the material recombination coefficients, and v_g is the group velocity.

From all information at t = t_0, i.e., F(t_o, z = 0 to L), B(t_o, z = 0 to L), N(t_o, z = 0 to L), and λ(t_0), the complex field distributions at t = t_o + Δt, i.e., F(t_o + Δt, z = 0 to L) and B(t_o + Δt, z = 0 to L), can be updated using (2), (12), and (13), and the carrier distribution of t = t_o + Δt, i.e., N(t_o + Δt, z = 0 to L), can be updated using (16). With this updated information, λ(t_o + Δt) can be obtained by finding the value at the minimum condition of Wronskian term. W(λ(t)) can be expressed as follows [16]:

$$W(\lambda(t)) = Det\,[T_{22}(t,L) + r_L T_{21}(t,L) - r_R T_{12}(t,L) - r_L r_R T_{11}(t,L)] \quad (17)$$

where $T_{mm(=1,2)}$(t, L) is a matrix element obtained from the overall transfer matrix [T(t = t_0+Δt, L)], and *Det* is the matrix determinant. In this equation, it is noted that Wronskian term will become T_{22}(t, L) at the condition of $r_L = r_R = 0$, like Davis's model.

The output power from the front-facet P_f, expressed in (18), is obtained by updating F(t, z = L) and λ(t)

$$P_f(t) = \frac{hc}{\lambda(t)} v_g A_4 |F(t, z = L)|^2 \quad (18)$$

where h is Plank constant and c is the velocity of light in free space. A_4 (= $d_4 w_4/\Gamma_4$) represent the effective cross-sectional area of an OWG (i.e., i = 4), and d and w are the thickness and width of the waveguide core layer, respectively.

The output wavelength λ_f(t) consists of the lasing wavelength λ(t) and the instantaneous wavelength shift $\Delta\lambda_{inst}$(t). They can be expressed by

$$\lambda_f(t) = \lambda(t) + \Delta\lambda_{inst}(t) \quad (19)$$

where

$$\Delta\lambda_{inst}(t) = -\frac{c}{\lambda^2(t=0)} \frac{d}{dt} \left[\text{Imag}\left(\ln\left(F(t, z = L)\right)\right)\right] \Big/ 2\pi \quad (20)$$

where Imag represents the imaginary part of complex value.

B. Changes of Absorption Coefficient and Refractive Index in EAM

Before performing an analysis of the EML, we must first estimate the absorption coefficient and refractive index change as a function of the applied voltage. Since these two parameters have a significant effect on the operational properties such as the output power, extinction ratio, and transient chirp, a careful design is required. When we apply reverse-biased voltage across the multiple-quantum well (MQW) of an EAM, the absorption at the lasing wavelength (located at the longer wavelength side of the absorption peak) is increased by the effect of a red-shift of the absorption peak and its broadening (i.e., quantum confined stark effect). To model this effect, we first analyzed the energy levels between the electron and holes in a conventional InGaAsP QW by solving the Schrödinger equation, which includes a Coulomb interaction by the exciton (i.e., exciton binding energy), and then utilized the absorption models for the exciton and continuum states [25]. In this model, the line-width broadening factors were used as fitting parameters. The absorption-induced refractive index change was obtained through the Kramers-Kronig relation [12].

Fig. 3 shows the calculated absorption spectra α_{absp} and the refractive index changes Δn_{absp} of the designed QW structure (i.e., 9.5 nm-thick QW with the bandgap wavelength of about 1.285 μm) for various values of the applied voltage. Absorption peak wavelength appears near the wavelength of 1.24 μm at zero bias voltage. As we intended, the absorption spectrum becomes red-shifted and broadened with the increase of. The calculated overall shapes in the absorption coefficient and refractive index change were similar to the measured ones in [7] except the wavelengths.

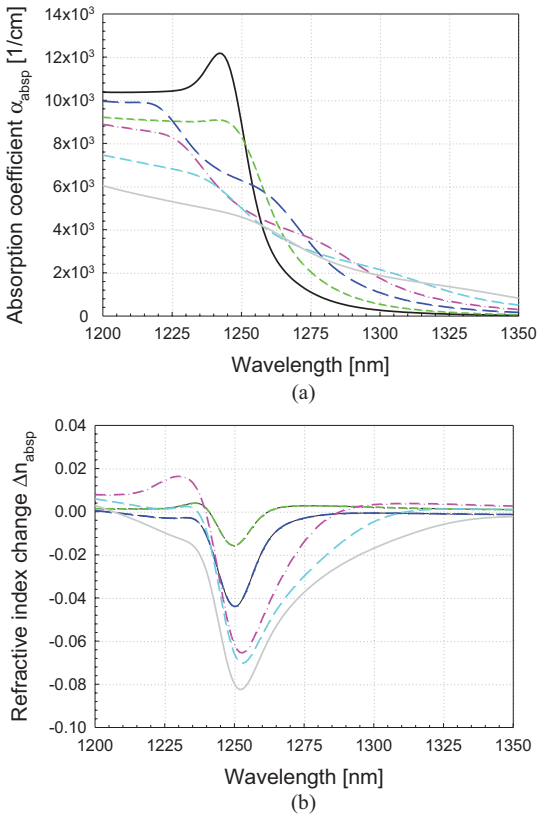

Fig. 3. (a) Calculated absorption spectra and (b) refractive index changes for various values of the applied voltage.

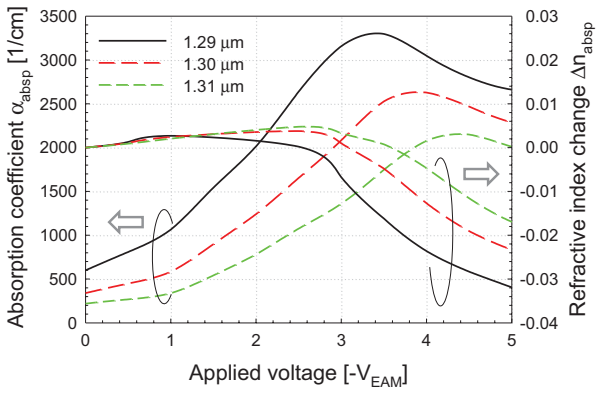

Fig. 4. Absorption coefficient and refractive index change for the wavelengths of 1.29 μm, 1.3 μm, and 1.31 μm as a function of the applied voltage of EAM.

Fig. 4 shows α_{absp} and Δn_{absp} for the wavelengths of near 1.3 μm as a function of $|-V_{EAM}|$. This figure indicates that, as the voltage increases, α_{absp} increases gradually to the saturation level, and Δn_{absp} increases slightly and then decreased rapidly. For the dependence on the operating wavelength, it is shown that, as the detuning decreases, the absorption coefficient at zero-bias voltage (i.e., the insertion loss of an EAM) increases, the ratio of absorption change with the voltage (i.e., the extinction ratio) increases, and the absorption-saturation voltage decreases. On the other hand, it is interesting to note that the negative slope of Δn_{absp} with the voltage (near the voltage $|-V_{EAM}|$ of 2.8 V) can induce negative chirp [18].

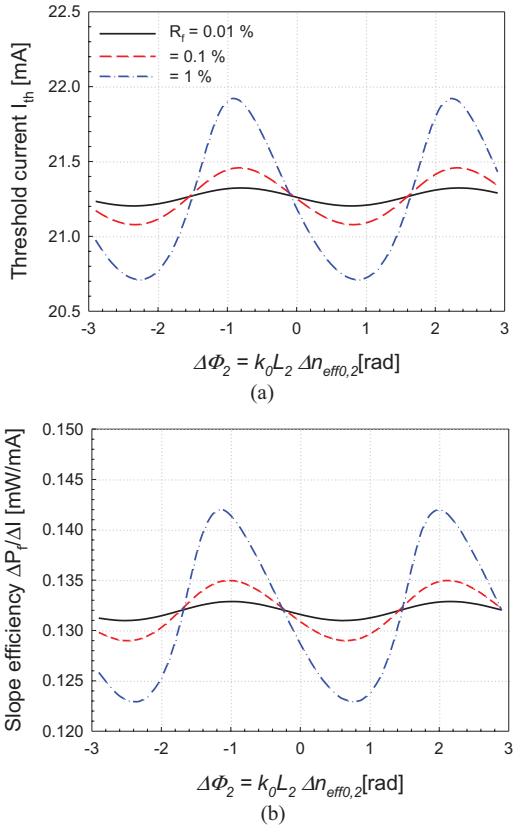

Fig. 5. Variations of (a) threshold current (I_{th}) and (b) slope efficiency ($\Delta P_f/\Delta I$) of the EML with κL_1 of 2 as a function of the phase parameter $\Delta\Phi_2$ for the output facet reflectivity R_f of 0.0%, 0.1%, and 1%. In this simulation, the voltage applied to an EAM V_{EAM} is 1.1 V, the current injected to the DFB laser I_{DFB} is 100 mA, and $\Delta\Phi_2/\Delta\ n_{eff0,2}$ is 966.64 rad.

III. Simulation Results

The optical light reflected from the output facet will experience the changes in the intensity (mainly by the output facet reflectivity and the absorption of an EAM) and in the phase (by the optical path length). This light will be coupled with the light emitted from the DFB laser and, as a result, changes the lasing (amplitude and phase) condition. To express the phase change of this reflected light effectively, we introduce a phase parameter $\Delta\Phi_2$ ($= k_0 L_2 \Delta n_{eff0,2}$, where k_0 is the wave number at a Bragg wavelength and $\Delta n_{eff0,2}$ is the refractive index change of region 2 (i.e., BWG)). The steady-state and large-signal analyses for the EMLs with the non-zero reflectivity at the output facet have been performed by numerical simulations using the parameters listed in Table I.

A. Simulation Results of Steady-State Analysis for EMLs

Fig. 4 shows the variations of threshold current I_{th} and slope efficiency $\Delta P_f/\Delta I$ of the EML with the normalized coupling coefficient κL_1 of 2 as a function of phase parameter $\Delta\Phi_2$ for the output facet reflectivity R_f of 0.01, 0.1, and 1%. The slope efficiency was obtained at the DFB current of 100 mA. The bias voltage of EAM is –1.1 V (i.e., off state of the EAM). This figure shows that, as the $\Delta\Phi_2$ is changed, I_{th} and $\Delta P_f/\Delta I$ are varied periodically, and these variations are larger with the

TABLE I
DEVICE PARAMETERS

Parameter	Value	Description
L_1	450 μm	Length of the DFB laser
L_2	200 μm	Length of the BWG
L_3	120 μm	Length of the EAM
L_4	80 μm	Length of the OWG
V	49.5 μm^3	Volume of the active region
Γ_1	0.08	Optical confinement factor of the DFB laser
Γ_2	0.512	Optical confinement factor of the BWG
Γ_3	0.15	Optical confinement factor of the EAM
A_4	1.375 μm^2	Effective area of the OWG
a_0	7.0×10^{-16} cm^{-2}	Linear differential gain
a_1	0.7×10^{14} cm^{-3}	Gain curvature
a_2	2.7×10^{-26} cm^3	Differential peak wavelength
r_L	0	Reflection coefficient of the rear facet
η	0.8	Injection efficiency
Λ	200.2 nm	Grating period
α_1	15 cm^{-1}	Internal loss of the active region
$\alpha_{2,4}$	10 cm^{-1}	Internal loss of the passive waveguide
N_0	2.0×10^{18} cm^{-3}	Transparent carrier density
ε	2.5×10^{-17} cm^3	Gain compression factor
A	1.2×10^{8} sec^{-1}	Linear recombination coefficient
B	1×10^{-10} cm^3/sec	Bimolecular recombination coefficient
C	4.5×10^{-29} cm^6/sec	Auger recombination coefficient
$n_{eff0,1}$	3.255	Effective refractive index of the DFB laser without a current injection
$n_{eff0,2}$	3.25 $+\Delta n_{eff0,2}$	Effective refractive index of the BWG
$n_{eff0,3}$	3.246	Effective refractive index of the EAM at $V_{EAM} = 0$ V
n_g	3.73	Group refractive index
a_H	3.2	Line-width enhancement factor

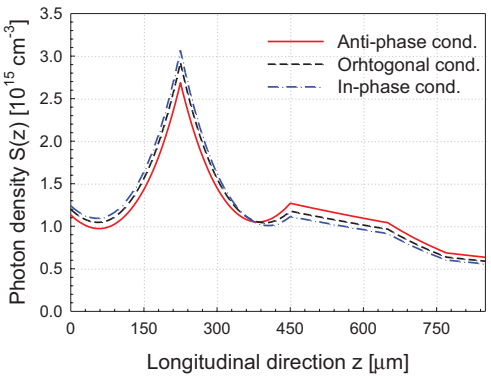

Fig. 6. Calculated longitudinal distributions of photon densities along the cavity S(z) for different phase conditions. In the simulation, R_f of 1%, V_{EAM} of –1.1 V, and I_{DFB} of 100 mA were used.

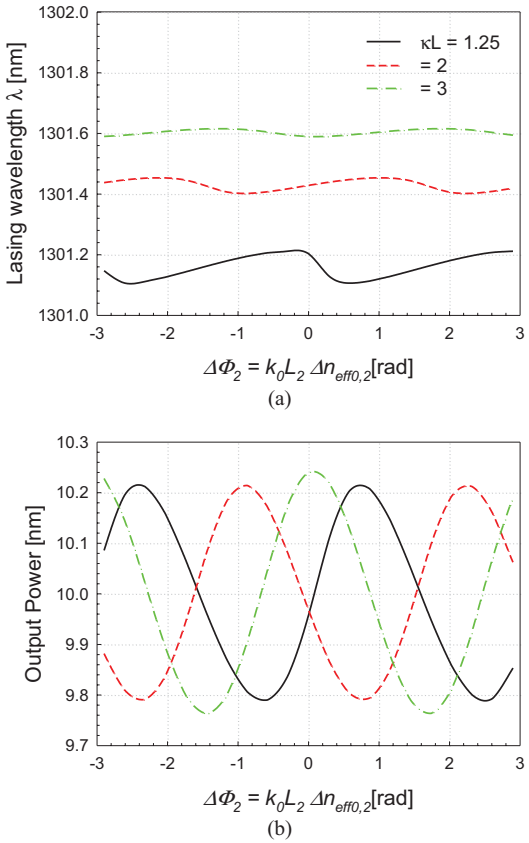

Fig. 7. Variations of (a) lasing wavelength and (b) output power for the EMLs with κL_1 of 1.25, 2, and 3 as a function of $\Delta\phi_2$. In the simulation, R_f of 1% is used.

increase of R_f. The period of these variations is about 2 rad where $\Delta n_{eff0,2}$ is changed to 2.07×10^{-3} at the L_2 of 200 μm.

For these variations with the phase parameter $\Delta\Phi_2$, they can be classified into three phase conditions: in-phase (which results in the decrease of the threshold current I_{th} and slope efficiency $\Delta P_f/\Delta I$ near $\Delta\Phi_2$ of 0.8 rad), anti-phase (the $\Delta\Delta\kappa$ increase of I_{th} and $\Delta P_f/\Delta I$ near $\Delta\Phi_2$ of –1 rad), and orthogonal condition (little change of I_{th} and $\Delta P_f/\Delta I$ near $\Delta\Phi_2$ of -0.2 rad). The slight differnece of $\Delta\Phi_2$ in each condition for different R_fs results from the variation of effective refractive index in the DFB laser due to the change of threshold carrier density. For each phase condition, the variation of I_{th} can be explained by the change of threshold condition in the DFB laser (i.e., the change of threshold carrier density). Fig. 5 shows the longitudinal distributions of photon densities along the cavity for different phase conditions. It is very interesting that the anti-phase condition (with higher I_{th}) provides the higher output power than the in-phase (with lower I_{th}) due to higher $\Delta P_f/\Delta I$. From this result, the variation of $\Delta P_f/\Delta I$ with respect to the phase conditon can be explained by the change of the effective reflectivity in between DFB laser and BWG (i.e., z = 450 μm). Therefore, we conclude

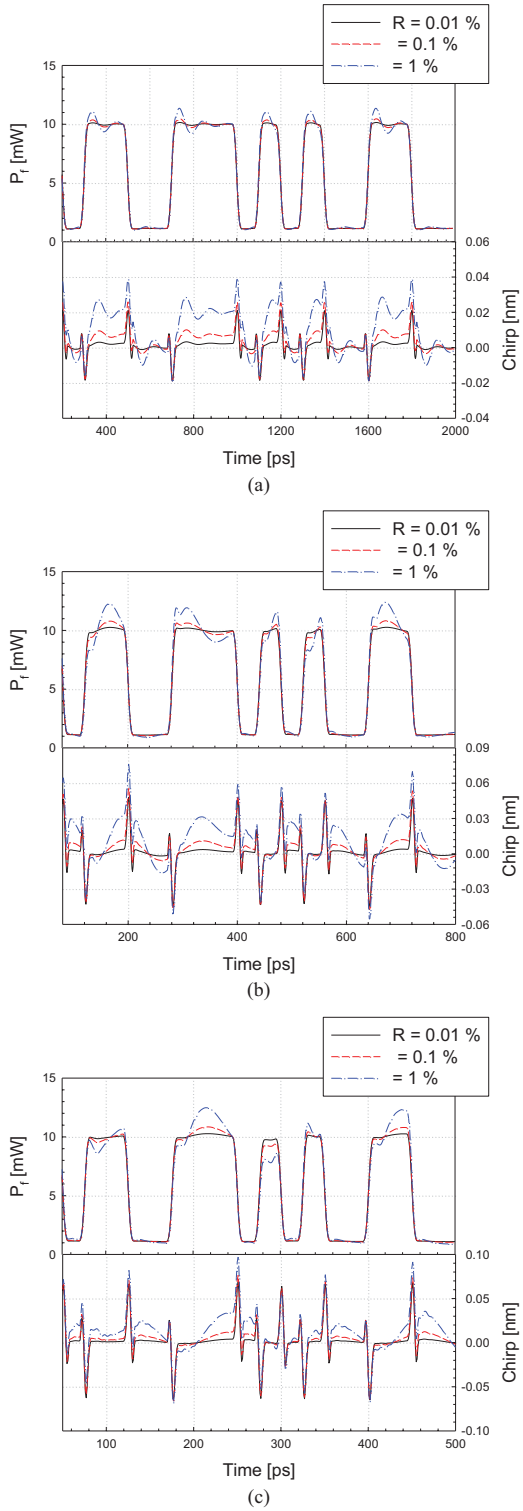

Fig. 8. Output power (upper) and chirp (lower) of the EML with κL_1 of 2 for output facet reflectivity R_f of 0.01%, 0.1%, and 1% at data rates of (a) 10 Gb/s, (b) 25 Gb/s, and (c) 40 Gb/s under in-phase condition.

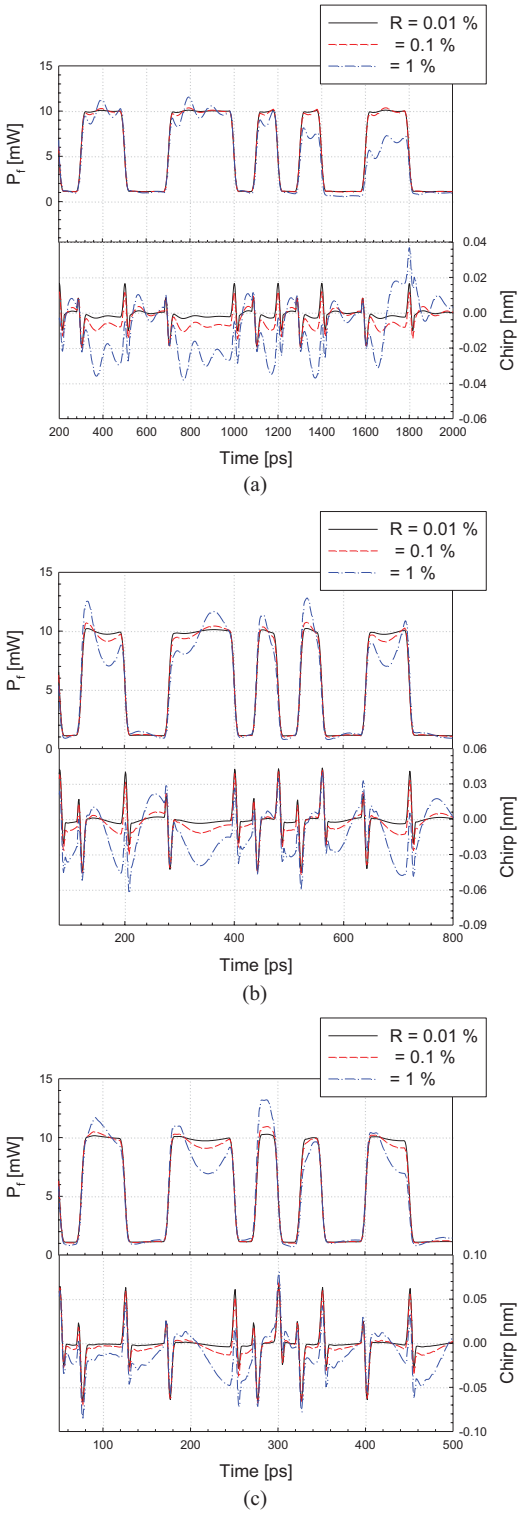

Fig. 9. Output power (upper) and chirp (lower) of the EML with κL_1 of 2 for output facet reflectivity R_f of 0.01%, 0.1%, and 1% at data rates of (a) 10 Gb/s, (b) 25 Gb/s, and (c) 40 Gb/s under anti-phase condition.

that the phase of the reflected light from the output facet can change the photon distribution along the cavity (which has an effect on $\Delta P_f/\Delta I$) as well as the threshold condition (I_{th}).

On the other hand, under the steady-stae analysis, it can be necessary to investigate the variations of the lasing wavelength and output power for the EML with different coupling coefficients since some other analysis based on the static model could explain the fact that high κL EMLs have high immunity to an external feedback [9].

Fig. 6 shows the lasing wavelength and output power of the EMLs with the normalized coupling coefficient κL_1 of 1.25, 2, and 3 as a function of $\Delta\Phi_2$. The injection current

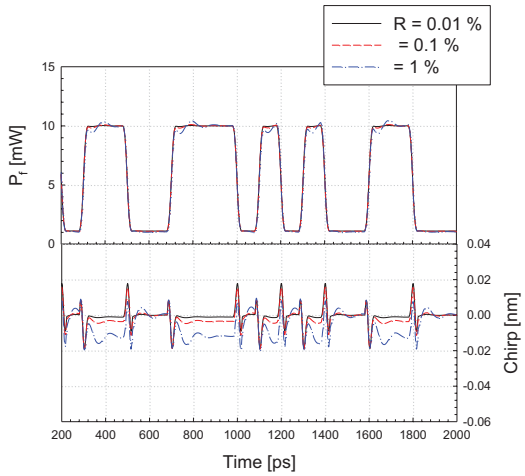

(a)

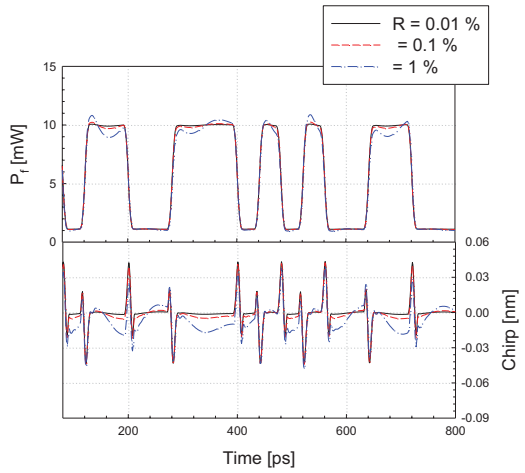

(b)

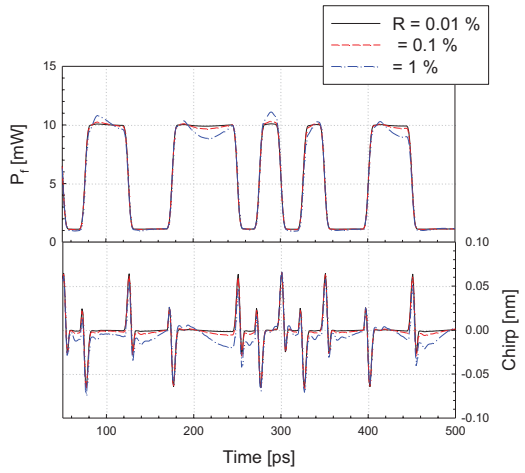

(c)

Fig. 10. Output power (upper) and chirp (lower) of the EML with κL_1 of 3 for output facet reflectivity R_f of 0.01%, 0.1%, and 1% at data rates of (a) 10 Gb/s, (b) 25 Gb/s, and (c) 40 Gb/s under anti-phase condition.

was adjusted for the averaged output power (i.e., the output power at zero output facet reflectivity) to be 10 mW. This figure indicates that, as κL_1 increases, the variation of lasing wavelength is considerably reduced (mainly due to the small variation of threshold carrier density), but that of the output power remains nearly unchanged except the phase difference.

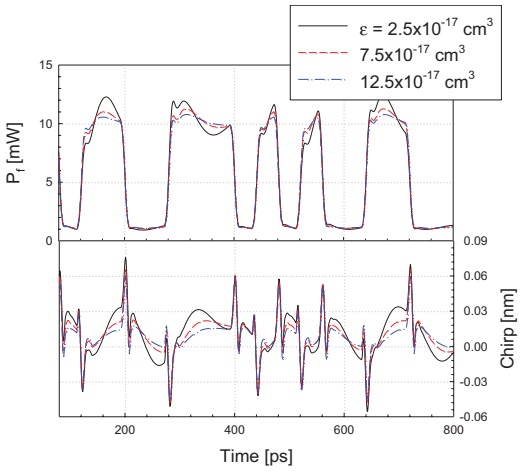

(a)

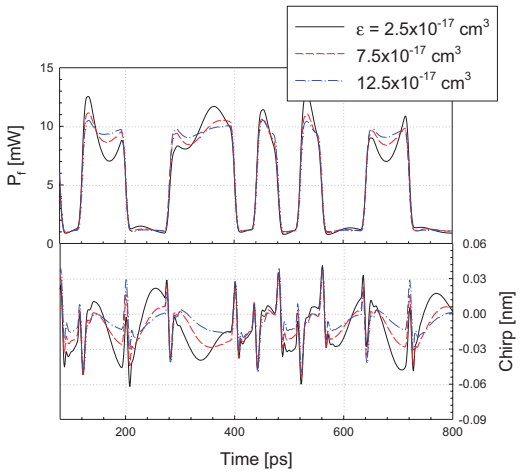

(b)

Fig. 11. Output power (upper) and chirp (lower) of the EML with κL_1 of 2 for various gain compression factors at the data rate of 25 Gb/s under (a) in-phase and (b) anti-phase conditions. In the simulation, R_f of 1% is used.

The reason for this unchanged power variation is that a high κL structure causes a large variation of the photon distribution even at the relatively small variation of the threshold carrier density (i.e. the threshold gain). From this result, we think that it is impossible for the analysis based on the static model to completely explain about the effect of the coupling coefficient on the feedback immunity.

B. Simulation Results of Large-Signal Analysis for EMLs

To perform the large-signal analysis, the voltage applied to the EAM was modulated with the raised cosine shape [15] (V_{p-p} = 1.8 V) and its rise and fall time was 25% of the pulse width. In this simulation, all initial values at t = 0 was obtained from the steady-state condition. The chirp $\Delta\lambda_f(t)$ was obtained from the relation $\Delta\lambda_f(t) = \lambda_f(t) - \lambda_f(t=0)$.

Fig. 7 and Fig. 8 show the output power and chirp of the EML with κL_1 of 2 for the R_f of 0.01, 0.1, and 1% at the data rate of 10, 25, and 40 Gb/s under the in- and anti-phase conditions, respectively. The phase parameter $\Delta\Phi_2$ of each phase condition was obtained by performing the steady-state analysis at the off state of the EAM (i.e. $V_{EAM} = -1.1$ V).

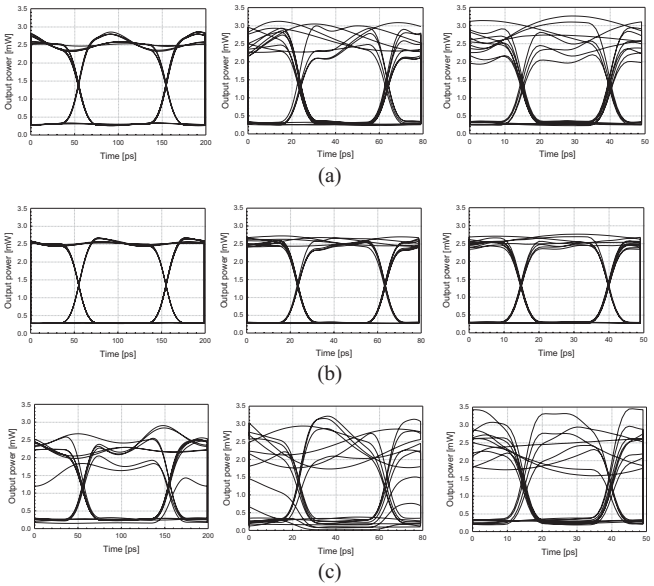

Fig. 12. Eye diagram of the EML with κL_1 of 2 at data rates of 10, 25, and 40 Gb/s under (a) in-phase, (b) orthogonal, and (c) anti-phase conditions. In the simulation, R_f of 1% is used.

For all data rates and phase conditions, as the R_f increases, the output power fluctuation and reflection-induced chirp (i.e., DFB chirp) are shown to be increased. The freqeuncy of these fluctuations (or ripples) was about 9 GHz which corresponds to the relaxation oscillation frequency of DFB laser. As the data rate (i.e., modulation speed) increses, the power fluctuation and transient chirp are also shown to be increased and, in particular, these tend to be seriously affected by the previous data patterns. In comparison between the in- and anti-phase conditions, the direction (or sign) of addiabtic chirp is opposite while that of transient chirp is the same. Besides, the output power fluctuation and chirp of the in-phase condtion are smaller than those of the anti-phase condtion at the same reflectivity.

Fig. 9 shows the output power and chirp of the EML with κL_1 of 3 under the same condition of Fig. 8. Compared to the results (of the EML with κL_1 of 2) shown in Fig. 8, the output power fluctuation and reflection-induced chirp are reduced considerably, unlike the steady-state analysis. For this result, something important to notice here is that the high κL structure contains large amounts of photon densities within the DFB region and, in particular, these photon densities are concentrated at phase-shift. These attributes in the high κL structure suppress the optical gain through nonlinear gain mechanism (i.e., gain suppression factor in (14)), which, in turn, increase the damping and weaken the relaxation oscillation under the modulation. Therefore, we can conclude that the main mechanism for the reduction of the power fluctuation and reflection-induced chirp (i.e., high immunity to external feedback) in the high κL structure is the damping effect due to $\kappa\kappa\kappa\kappa$ the gain saturation. From this point of view, such reductions of the in-phase condition can also be explained by an increase in the gain saturation resulting from the increase of photon densities within the DFB region, as shown in Fig. 5.

As a result, it is expected that a high damping structure can be realized by increasing the gain compression factor itself. To confirm this, we examined the dependence on the gain compression factor for the EMLs with the same κL_1. Fig. 10 shows the output power and chirp of the EML with κL_1 of 2 for the various gain compression factors at a data rate of 25 Gb/s under the in- and anti-phase conditions. As we expected, it is clearly shown that, as the gain compression factor increases, the output power fluctuation and DFB chirp are reduced.

Fig. 11 shows eye diagrams of the EML with κL_1 of 2 at the data rate of 10, 25, and 40 Gb/s under the in-phase, orthogonal, and anti-phase conditions. This figure shows that, as the data rate increases, the fluctuations of 1's level in the output power κincrease. In particular, relatively larger fluctuations are shown under the anti-phase condition. Under the orthogonal condition, low fluctuations of 1's level (i.e., clear eye openings) appear even at the output reflectivity R_f of 1%. This is very interesting result. When we realize the phase control section (PCS) within the BWG, it is possible to control to be operated at this condition. For the conventional EML without this PCS, it can also be observed experimentally by finding the cetrain operating condition (i.e., the current of DFB laser or the voltage of EAM) in which a clear eye pattern appears at the relatively high reflectivity (i.e. $R_f \sim 1\%$).

IV. Conclusion

We investigated the effects of the residual facet reflection on the static and dynamic properties of the EML theoretically. For this analysis, we developed the accurate and consistent time-domain transfer-matrix-based laser model of the EML. Based on this model, we performed the steady-state and large-signal analysis for the EML with the non-zero output facet reflectivity for the various device parameters and operational conditions. It was found that the EML having a high gain compression factor can reduce the power fluctuation and facet reflection-induced chirp under the large-signal modualtion, which results from the increase of damping effect of DFB laser. As for the realization of the high damping laser, we think that it can be desirable to use the quantum dot (or dash) as an active region in DFB laser or to design the active region (i.e., quantum well and separate-confinement hetero-structure (SCH) layer) which can provide high damping [11], [26]. In addition, through these simulation, various distinctive features were found as follows:

1) The optical light reflected from the output facet changes the longitudinal distribution of photon densities along the cavity (above threshold condition) as well as the threshold carrier density (i.e., threshold condition) through the variation of its phase. As a result, these changes cause the variations in the slope efficiency (via the photon distribution) and threshold current (via the carrier density).
2) In comparison between in- and anti-phase conditions between this reflected light and the light emitted from the DFB laser, the direction (or sign) of adiabatic chirp was opposite while that of transient chirp was the same. In particular, under the anti-phase condition, relatively

higher output power was obtained at the same DFB current under the steady-state but larger power fluctuation was shown at the same averaged output power (i.e., the output power at zero output facet reflectivity) under the large-signal modulation.

3) For the same device structure, as the modulation speed (i.e., data rate) incresed, the power fluctuation and transient chirp were increased and tended to be more affected by the previous data patterns.
4) As the κL increases, the power fluctuation and reflection-induced chirp were considerably reduced under the large-signal modulation. For this result, it was identified that such a reduction is originated from the increase of the damping due to the gain saturation.
5) Under the orthogonal condition, a clear eye opening appears even at the output reflectivity R_f of 1 %.

REFERENCES

[1] *IEEE 802.3ba 40 Gb/s and 100 Gb/s Ethernet Task Force Public Area*. (2010, Jun. 19) [Online]. Available: http://www.ieee802.org/3/ba/index.html

[2] T. Fujisawa, S. Kanazawa, N. Nunoya, H. Ishii, Y. Kawaguchi, A. Ohki, N. Fujiwara, K. Takahata, R. Iga, F. Kano, and H. Oohashi, "4×25-Gbit/s, 1.3-mm, monolithically integrated light source for 100-Gbit/s Ethernet," in *Proc. Eur. Conf. Opt. Commun.*, 2010, no. Th.9.D.1, pp. 1–6.

[3] M. Yamaguchi, T. Kato, T. Sasaki, K. Komatsu, and M. Kitamura, "Requirements for modulator-integrated DFB LD's for penalty-free 2.5-Gb/s transmission," *J. Lightw. Technol.*, vol. 13, no. 10, pp. 1948–1954, Oct. 1995.

[4] J.-S. Choe, Y.-H. Kwon, J.-S. Sim, and S.-B. Kim, "40 Gb/s electroabsorption modulated DFB laser with tilted facet formed by dry etching," *Semicond. Sci. Technol.*, vol. 22, no. 7, pp. 802–805, Jul. 2007.

[5] Y. H. Kwon, J. S. Choe, J. S. Sim, S. B. Kim, H. Yun, K. S. Choi, B. S. Choi, and E. S. Nam, "40 Gb/s traveling-wave electroabsorption modulator-integrated DFB lasers fabricated using selective area growth," *ETRI J.*, vol. 31, no. 6, pp. 765–769, Dec. 2009.

[6] C. Sun, B. Xiong, J. Wang, P. Cai, J. Xu, J. Huang, H. Yuan, Q. Zhou, and Y. Luo, "Influence of residual facet reflection on the eye-diagram performance of high-speed electroabsorption modulated lasers," *J. Lightw. Technol.*, vol. 27, no. 15, pp. 2970–2976, Aug. 2008.

[7] M. Aoki, S. Takashima, Y. Fujiwara, and S. Aoki, "New transmission simulation of EA-modulator integrated DFB-lasers considering the facet reflection-induced chirp," *IEEE Photon. Technol. Lett.*, vol. 9, no. 3, pp. 380–382, Mar. 1997.

[8] B. H. Park, I. Kim, B.-K. Kang, Y.-D. Bae, S.-M. Lee, Y. H. Kim, D.-H. Jang, and T.-I. Kim, "Investigation of optical feedback in high speed electroabsorption modulated lasers with a window region," *IEEE Photon. Technol. Lett.*, vol. 17, no. 4, pp. 777–779, Apr. 2005.

[9] R. A. Salvatore and R. T. Sahara, "Reduction in reflection-induced chirp from photonic integrated sources," *IEEE Photon Technol. Lett.*, vol. 14, no. 12, pp. 1662–1664, Dec. 2002.

[10] H. Soda, Y. Kotaki, H. Sudo, H. Ishikawa, S. Yamakoshi, and H. Imai, "Stability in single longitudinal mode operation in GaInAsP/InP phase-adjusted DFB lasers," *IEEE J. Quantum Electron.*, vol. 23, no. 6, pp. 804–814, Jun. 1987.

[11] L. A. Coldren and S. W. Corzine, *Diode Lasers and Photonic Integrated Circuits*. New York: Wiley, 1995.

[12] L. M. Zhang and J. E. Carroll, "Semiconductor 1.55 mm laser source with gigabit/second integrated electroabsorptive modulator," *IEEE J. Quantum Electron.*, vol. 30, no. 11, pp. 2573–2577, Nov. 1994.

[13] B. S. Kim, Y. Chung, and S. H. Kim, "An efficient split-step time-domain dynamic modeling of DFB/DBR laser diodes," *IEEE J. Quantum Electron.*, vol. 36, no. 7, pp. 787–794, Jul. 2000.

[14] M. G. Davis and R. F. O'Dowd, "A transfer matrix method based large signal dynamic model for multielectrode DFB lasers," *IEEE J. Quantum Electron.*, vol. 30, no. 11, pp. 2458–2466, Nov. 1994.

[15] Y. Kim, H. Lee, J. Lee, J. Han, T. W. Oh, and J. Jeong, "Chirp characteristics of 10-Gb/s electroabsorption modulator integrated DFB lasers," *IEEE J. Quantum Electron.*, vol. 36, no. 8, pp. 900–908, Aug. 2000.

[16] T. Makino, "Transfer-matrix formulation of spontaneous emission noise of DFB semiconductor lasers," *J. Lightw. Technol.*, vol. 9, no. 1, pp. 84–91, Jan. 1991.

[17] O. K. Kwon, Y. A. Leem, D. H. Lee, C. W. Lee, Y. S. Baek, and Y. C. Chung, "The effects of asymmetric grating structures on output efficiency and single longitudinal mode operation in l/4-shifted DFB laser," *IEEE J. Quantum Electron.*, vol. 47, no. 9, pp. 1185–1194, Sep. 2011.

[18] H. Fukano, Y. Akage, Y. Kawaguchi, Y. Suzaki, K. Kishi, T. Yamanaka, Y. Kondo, and H. Yasaka, "Low chirp operation of 40 Gbit/s electroabsorption modulator integrated DFB laser module with low driving voltage," *IEEE J. Sel. Topics Quantum Electron.*, vol. 13, no. 5, pp. 1129–1134, Sep.–Oct. 2007.

[19] S. Makino, K. Shinoda, T. Kitatani, H. Hayashi, T. Shiota, S. Tanaka, M. Aoki, N. Sasada, and K. Naoe, "High-speed EA-DFB laser for 40-G and 100 Gb/s," *IEICE Trans. Electron.*, vol. E92-C, no. 7, pp. 937–941, Jul. 2009.

[20] G. L. Li, C. K. Sun, S. A. Pappert, W. X. Chen, and P. K. L. Yu, "Ultraspeed traveling-wave electroabsorption modulator-design and analysis," *IEEE Trans. Microw. Theory Tech.*, vol. 47, no. 7, pp. 1177–1183, Jul. 1999.

[21] O. K. Kwon, Y. T. Han, Y. S. Baek, and Y. C. Chung, "Improvement of modulation bandwidth in electroabsorption-modulated laser by utilizing the resonance property in bonding wire," *Opt. Exp.*, vol. 20, no. 11, pp. 11806–11812, May 2012.

[22] H. Ghafouri-Shiraz, *Distributed Feedback Laser Diodes and Optical Tunable Filters*. New York: Wiley, 2003.

[23] J. Skagerlund, F. Pusa, O. Sahlèn, L. Gillner, R. Schatz, P. Granestrand, L. Lundqvist, B. Stoltz, J. Terlecki, F. Wahlin, A.-C. Mörner, J. Wallin, and O. Öberg, "Evaluation of an automatic method to extract the grating coupling coefficient in different types of fabricated DFB lasers," *IEEE J. Quantum Electron.*, vol. 34, no. 1, pp. 141–146, Jan. 1998.

[24] P. Correc, "Stability of phase-shifted DFB lasers against hole burning," *IEEE J. Quantum Electron.*, vol. 30, no. 11, pp. 2467–2476, Nov. 1994.

[25] P. J. Steven, M. Whitehead, G. Parry, and K. Woodbridge, "Computer modeling of the electric field dependent absorption spectrum of multiple quantum well material," *IEEE J. Quantum Electron.*, vol. 24, no. 10, pp. 2007–2016, Oct. 1988.

[26] W. F. Sharfin, J. Schlafer, W. Rideout, B. Elman, R. B. Lauer, J. LaCourse, and F. D. Crawford, "Anomalously high damping in strained InGaAs-GaAs single quantum well lasers," *IEEE Photon. Technol. Lett.*, vol. 3, no. 3, pp. 193–195, Mar. 1991.

Oh Kee Kwon received the B.S. and M.S. degrees in electronic engineering from Hanyang University, Korea, in 1996 and 1998, respectively, and the Ph.D. degree in electrical engineering from the Korea Advanced Institute of Science and Technology, Daejeon, Korea, in 2012.

He joined the Basic Research Laboratory, Electronics and Telecommunications Research Institute, Daejeon, in 2002, where he has been engaged in the research and development of a wavelength tunable laser, wavelength selective switch, and high-speed EML array. His current research interests include design and development of external cavity tunable lasers with fast tuning speed and broad tuning range.

Yong Soon Baek received the B.S. degree in physics from Seoul National University, Seoul, Korea, in 1991, and the Ph.D. degree in nonlinear optics from the Center for Research and Education in Optics and Lasers, University of Central Florida, Orlando, in 1997.

He joined the Basic Communication Research Laboratory, Electronics and Telecommunications Research Institute, Daejeon, Korea, in 1999. He has been engaged in research on developing semiconductor optical amplifiers-related functional devices, optical transceivers for fiber-to-the-home applications, and advanced optical switches for reconfigurable optical add-drop multiplexer systems. His current research interests include development of 100 Gb/s Ethernet transceiver modules.

Yun C. Chung (S'81–M'83–SM'03–F'06) is a Professor of electrical engineering with the Korea Advanced Institute of Science and Technology, Daejeon, Korea, since 1994. From 1987 to 1994, he was with the Lightwave Systems Research Department, AT&T Bell Laboratories, Murray Hill, NJ. From 1985 to 1987, he was with the Los Alamos National Laboratory, Los Alamos, NM, under the AWU-DOE Graduate Fellowship Program. He is over the author or co-author of more than 400 journal and conference papers and holds more than 60 patents. His current research interests include high-capacity wavelength-division-multiplexing (WDM) transmission systems, all-optical WDM networks, optical performance monitoring techniques, WDM passive optical networks, and fiber-optic networks for wireless communications.

He is a fellow of the Optical Society of America. He is a member of the Korean Academy of Science and Technology.